Modulation of fMRI signal by respiratory activity

Rui José Pereira Bastos

Instituto Superior Técnico, Lisboa, Portugal

November 23, 2016

Abstract

This study aims to investigate how the blood oxygen level dependent (BOLD) signal measured with fMRI at ultrahigh field (7 Tesla) is modulated by respiratory activity. This is done with BOLD-fMRI data from a pilot study collected simultaneously with cardiac, respiratory, and endtidal CO_2 pressure recordings, from two volunteers performing two tasks: 1) paced breathing (PB): cued inspiration/expiration at short vs long pace; and 2) number generation (NG): sequential count down vs random number generation. Testing of the physiological data showed that the volunteers did not comply with the experimental protocol during most of the time. A first analysis was performed by employing a general linear modeling (GLM) approach applied to the BOLD timecourse of each voxel with the regressors based on the physiological recordings and task-periods. These were convolved with the respective haemodynamic response functions and used in the GLM. The results obtained showed relatively significant activation in a region of the brainstem (the pons) possibly coincident with the pneumotaxic center. Another approach was devised that performed a GLM analysis replacing the task-related regressors with the respiratory rhythm. These revealed significant results in the brainstem region: a visible cluster possibly identifiable as the dorsal raphe, a nucleus involved in the motor action of respiration; a second cluster not clearly identified, situated in the thin boundary region between the pons and the medulla oblongata; a third very consistent cluster in the pons region identified with the pneumotaxic center, one of the centers responsible for generating the respiratory rhythm; and several other regions of consistent activation, namely in the cerebellum, that require further study. The conclusions are promising, and the approach of using this set of regressors shows relevant results, despite the low number of datasets. A more thourough study is therefore feasible, after optimization of the approaches followed in this work, and is expected to provide statistical significance to the preliminary results found in this work.

Keywords: fMRI, general linear modeling, physiological noise, respiration, brainstem.

1. Introduction

The knowledge of the brain and its functioning has been greatly increasing in the last years. A good part of this rhythm of development is due to Magnetic Ressonance Imaging (MRI) technologies, with functional MRI (fMRI) gaining more and more relevance.

The objective of this thesis is to investigate the effects of respiration on high-spatial-resolution Blood-oxygen-level dependent contrast imaging (BOLD)-fMRI data and to localize respiration-related BOLD-fMRI activity, using data from a pilot study of two healthy volunteers, who underwent two tests while inside the scanner.

1.1. Respiration

Respiration is an essential physiological mechanism: it begins the process of oxygenation of the tissues and is extremely relevant in keeping the human

body free of the build up of some toxic substances, namely carbon dioxide (CO_2) [11]. The underlying mechanism must provide both stability and responsiveness to respiration, so as to allow it to adjust to physical and chemical disturbances and coordinate with other air flow generating movements.

The origin of respiration is widely considered to be in a region of the brainstem called the preBötzinger complex (preBötC) [9, 10] although there still exists some debate over the specific details [10]. There are also some respiratory nucleus present in the medulla, in dorsal and ventral groups, but lesions in these areas do not stop respiratory activity [11].

Some studies pose that respiratory rhythm generation is provided by the coupling of two distinct groups of neurons: the previously mentioned preBötC and the retrotrapezoid nucleus (RTN) [9]. The RTN was found to apparently overlap the parafacial respiratory group (pFRG), with both sometimes being mentioned as being the same structure, driving researchers to refer to their general region as the RTN/pFRG [10] until it is known if they are anatomically and functionally distinct nuclei. Both these structures, the preBötC and the pFRG/RTN are accepted as the main respiratory rhythm generators, working as coupled oscillators, with the first generating inspiratory rhythm, and the second generating expiratory activity [9].

The literature describes the full control of respiration as being based around the medullary groups, the pFRG/RTN and the preBötC. The rhythms generated by these regions are then modulated by various regions in the brainstem, including the pons. The physical actions that lead through inspiration and expiration are formed by the premotor and motor efferent networks, which include interneurons both in the brainstem and in the spinal cord [13].

1.2. Functional Magnetic Resonance Imaging

FMRI, like MRI, works on the assumption that certain nuclei, like hydrogen, have an intrinsic magnetic moment, and that when subjected to a magnetic field B_0 they rotate at a certain frequency, which is proportional to the field strength and gives them a certain angular momentum [4].

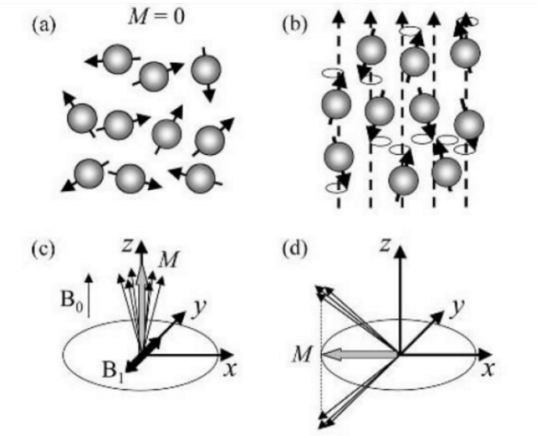

Figure 1: Behavior of a proton sample when placed in a strong magnetic field; a) When no magnetic field is applied, the magnetic moments are randomly oriented, yielding zero net magnetization; b) When a static magnetic field B_0 is applied, the moments align either parallel or anti-parallel to the field. The parallel configuration is slightly less energetic, hence a non-zero M vector is generated; c) A oscillating magnetic field B_1 changes the orientation of the nuclear moments until there is a measurable magnetization in the transversal xy plane (d) [15].

The lone proton angular momentum is quantized in the magnitude of the z component (parallel to B_0), meaning that it can only be parallel or antiparallel to the direction of the magnetic field. The NMR signal is obtained when there are transitions between these two levels, which must be induced by an external energy source, provided by a radiofrequency (RF) pulse. The RF pulse is applied at the resonance frequency (known as the Larmor frequency), in order to carry the energy that corresponds exactly to the gap between those two levels [24].

After a 90 RF pulse, we have an arbitrary magnetization vector with a non-zero $M_{xy}(0)$ and $M_z(0) = 0$. At later times, these magnitudes are described by the Bloch equations:

$$M_{xy}(t) = M_{xy}(0)e^{-\frac{t}{T_2}} \quad (1)$$

$$M_z(t) = M_0(1 - e^{-\frac{t}{T_1}}) \quad (2)$$

where T_1 is spin-lattice constant and T_2 is the spin-spin constant. They both describe relaxation along some direction relative to B_0: T_1 along the direction of the magnetic field, arising from differences in the local environment; and T_2 along the plane perpendicular to B_0, arising from interactions with neighboring nuclei. There is a third constant, T_2^*, used when some other effects that influence the transversal relaxation, namely the intrinsic magnet design and the differences in magnetic susceptibilities between different tissues, both of which will cause spatial variations in the strength of the magnetic field [15].

The knowledge that different tissues have different values of these constants is essential to create contrast in the MRI images, which are usually formed by spin-warping imaging. This consists of two steps, phase-encoding and frequency-encoding, both based on the use of linear magnetic field gradients [17].

fMRI is then achieved by acquiring sucessive MRI images, and relying on the sensitivity of the NMR signal to the concentration of oxygen in the blood inside the brain, a mechanism called BOLD effect [15]. It is specially noticeable when the technique used is sensitive to T_2^*, such as gradient recalled echo (GRE) [4]. The mechanism depends on a localized increase in neural activity, which leads to local vasodilatation and thus an increase in blood flow, which obviously means an increase in oxygen delivery. The rate of oxygen consumption, however, does not increase proportionaly [7, 19]. As a result, there will be an excess of oxygenated hemoglobin relative to deoxyhemoglobin, and while the first is diamagnetic, along with the surrounding tissue, the second is paramagnetic [24]. This will have an effect in the local magnetic field gradients, and since image contrast in T_2^*-weighted measurements depends on changes in the local magnetic susceptibility [15], there will be noticeable differences in the images acquired due to brain activation [24].

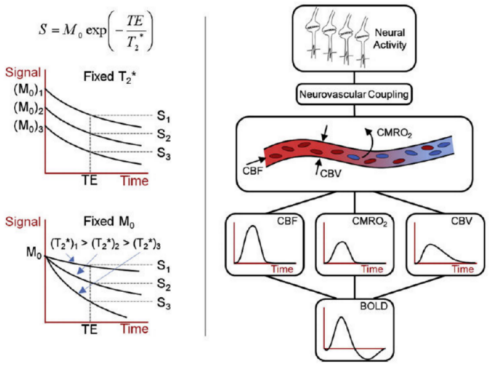

Figure 2: Origins of the BOLD signal; (Left) Dependence of the measured BOLD signal's magnitude on the initial magnetization, M_0, and the decay T_2^*. (Right) Schematic representation of the chain process leading to the measured BOLD signal [2].

It is obvious that if there is any phenomenon that alters the brains' vascular processes, the BOLD signal will no longer accurately depict neuronal activation. It is what happens with cardiac and respiratory effects, which introduce correlated changes in the BOLD signal that might not be related to neuronal activation [17]. The same happens in reaction to CO_2 levels, since this substance is a powerful vasoactive substance, leading to vasodilation in hypercapnia and vasoconstriction in hypocapnia. This means that taking into account its effects in the BOLD signal is extremely relevant during tests oriented to assess respiratory activity [22].

1.3. Physiological noise

Physiological sources of noise are a special component of noise, both in the sense that they consist of limitations to the imaging intrinsic to the human body and physiology in themselves, and by sometimes encompassing things like motion artifacts [17]. In this work, physiological noise is understood as those fluctuations in the BOLD signal produced by physiological mechanisms that somehow affect the blood flow, blood volume and blood oxygen concentration, and hence contribute as sources of the BOLD effect additionally to neuronal sources of interest.

The most relevant of these are probably cardiac and respiratory induced mechanisms, like arterial pulsatility [16] and changes in B_0 [18] and arterial PCO_2 [25]. Because physiological noise can mask neural activity underlying BOLD changes, several strategies have been developed for modeling and removing it.

It has been shown that non-periodic HR fluctuations have a significant spurious impact on the BOLD signal [20]. Respiratory Volume per Time (RVT), or the amount of air inspired with each breath , has been proposed as a surrogate for the end-tidal CO_2 concentration, and was originally defined by Birn as as the ratio of the difference between the maximum and minimum belt positions at inspiration and expiration peaks, respectively, and the length interval [3]. $P_{ET}CO_2$ has been correlated with RVT variations [3, 6], but the BOLD signal variations accounted by these two variables are not completely identical [6].

1.4. General Linear Model

The GLM is a linear model generally depicting a timecourse of the fMRI data as a weighted sum of basis functions (so called regressors) and some measure of noise, and then fits it to the data by estimating the weights. The simple formulation is the following:

$$y(t) = \beta X(t) + \epsilon(t) \tag{3}$$

where $y(t)$ is an N-sized vector, β is a P-sized vector with the weights, $X(t)$ is a NxP matrix (called the design matrix) that contains the P regressors whose contributions are to be estimated, and $\epsilon(t)$ is an N-size vector containing the residuals [15]. These residuals are usually modelled as an independently and identically distributed Gaussian random variable [26]. This allows for the problem to be solved by an Ordinary Least Squares approach, which consists of minimizing the squared residuals.

2. Methods

It has been shown that during regular awake respiration there is brainstem activity related to respiration and that this activity is modulated with the increasing of respiration frequency caused by a cognitive task, more specifically, random number generation [8]. There have also been studies exploring the relation between paced breathing and hypocapnic cerebrovascular reactivity (CVR) and its effect in the BOLD mechanism [22].

2.1. Test Protocol

The two tasks were defined as follows: **Paced Breathing (PB)**, paced breathing, following inspiration/expiration cues, at relatively short/fast (A1) and long/slow (A2) pace, intercalated with spontaneous normal breathing (B) [22]; and **Number Generation (NG)**, random number generation (A1) and sequential count down (A2), intercalated with spontaneous normal breathing (B) [8]. The order and timings of the A1, A2 and B conditions for each PB and NG protocol are shown in Table 1.

Outside the scanner, the subject was instructed about the experiment, $P_{ET}CO_2$ measurements were performed for calibration of the capnograph, and then the subject performed one PB and one NG task, for practice. Two PB tasks and one NG task were performed inside the scanner, during fMRI acquisition, in the following order: PB1, NG, PB2.

2.2. Data acquisition

The data was acquired on a 7 T Siemens whole-body scanner equipped with a custom-built 32-channel receive birdcage RF coil, at the Athinoula A. Martinos Center for Biomedical Imaging. Two healthy volunteers underwent a structural imaging scan and then performed a sequence of three 5 minute tasks while undergoing an fMRI scan, with cardiac and respiratory data being simultaneously recorded.

2.3. Image acquisition

fMRI data was acquired with a simultaneous multi slice (SMS) gradiend-echo echo planar imaging (EPI) sequence performed, with TE = 32 ms, TR = 2500 ms, and flip angle = 75∘. Whole-brain 1.1 mm isotropic images were collected, covering 123 sagittal slices with FOV = 264 x 198 mm^2. Slices

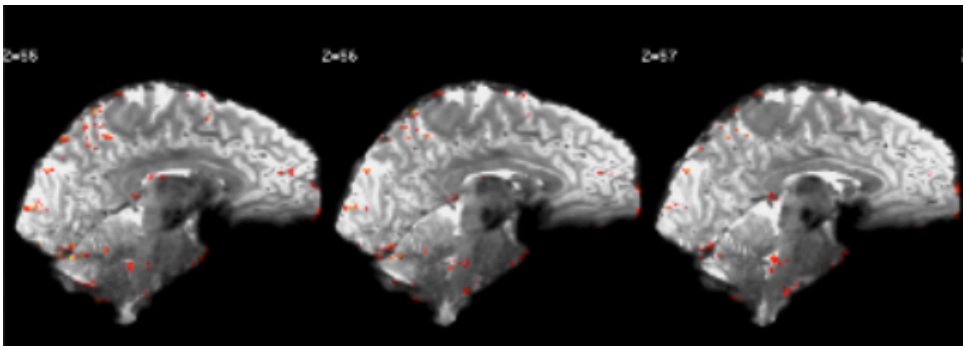

Figure 3: RR activation map for subject 1 performing task PB1 (sagittal slices from y = 55 to y = 57).

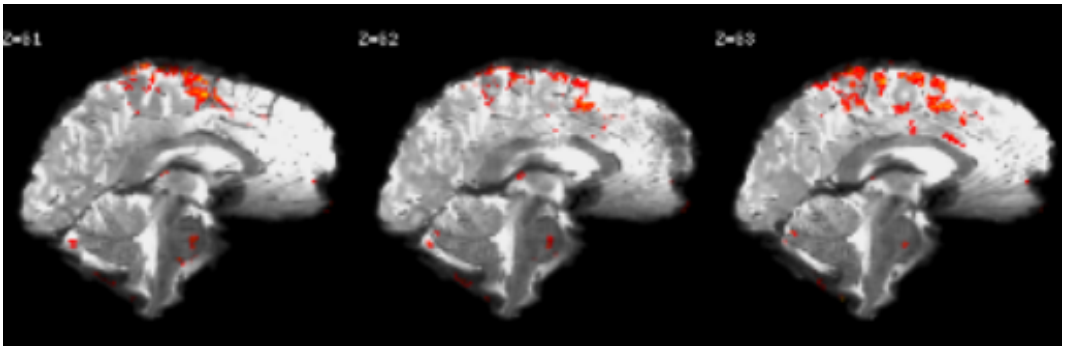

Figure 4: RR activation map for subject 2 performing task NG (sagittal slices from y = 61 to y = 63).

were acquired in an interleaved order with a Generalized Autocalibrating Partially Parallel Acquisition (GRAPPA) acceleration factor of 3. Acquisition time for all fMRI experiments was 390 s, i.e., approximately 6 min and 30 s (corresponding to a total of 156 volumes). Whole-brain T1-weighted structural images were also obtained from each subject during the scanning sessions using an MPRAGE sequence [23]

2.4. Physiological recordings

The subjects' cardiac data was recorded using a pulse transducer (TN1012/ST, ADInstruments) placed on the left index finger. Respiratory data was measured with a pneumatic belt (UFI Model 1132 Pneumotrace II, UFI) strapped around the subjects' upper abdomen. $P_{ET}CO_2$ data were recorded with a capnograh. All traces, along with a trace signaling the MRI scan triggers (one per volume TR), were acquired with a sampling rate of 1000 Hz.

2.5. Preprocessing

Preprocessing of the fMRI images was achieved through the process optimized by Nunes [17]. The tools used were the ones available in the Oxford Center for fMRI of the Brain (FMRIB) Software Library (FSL, 5.0 version) [21, 14]. A gray matter mask was also obtained through registration of the subjects' data with the MNI 152 standard space.

2.6. Cardiac trace

The waveform obtained through the pulse transducer was used to determine the cardiac cycle phase and the cardiac rate at the time instant corresponding to the center of the TR interval during which each fMRI volume was acquired. The pulse transducer signal (cardiac signal) was first band-pass filtered using a two-way least-squares Finite Impulse Response (FIR) filter with cutoff frequencies fc_{lower} = 0.5 Hz and fc_{upper} = 1.7 Hz, to yield a smoothed version of the signal preserving its fundamental frequency (typically around 1 Hz) but removing lower frequency trends and higher frequency fluctuations which introduce undesirable fluctuations and lead

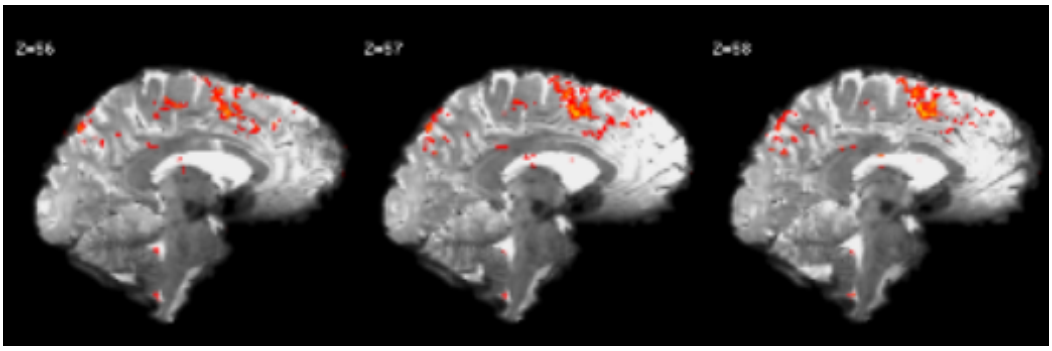

Figure 5: RR activation map for subject 2 performing task PB2 (sagittal slices from z = 56 to z = 58).

B	A1	B	A2	B	A1	B	A2	B	A1	B	A2	B
30 s	30 s	30 s	30 s	30 s	30 s	30 s	30 s	30 s	30 s	30 s	30 s	30 s

Table 1: Protocol timings: B is normal breathing, A1 is Action 1 and A2 is Action 2.

to false detection of R peaks (false positives).

2.7. Respiratory volume trace

The respiratory waveform was used to compute the respiratory rate (RR) for each fMRI volume, as well as the RVT [3]. Similarly to the cardiac signal, computing the respiratory rate relies on peak detection and follows the same general principles. Low-pass filtering was carried out using the same FIR filter to remove undesirable noise fluctuations, only this time a lower cutoff frequency $f_c = 1$ Hz was used to adjust for the typically lower respiratory frequency (around 0.3 Hz) and preserve the main signal waveform. Contrary to the cardiac signal, where only the peaks were of interest, the amplitude of the waveform is also a concern and should be preserved after filtering, in order to compute the RVT.

2.8. PETCO2 trace

End tidal partial pressure of CO_2 level was measured with a capnograph, which has an intrinsic delay due to the time taken for air to travel from the mouth to the CO_2 sensor. This delay was previously estimated as, on average, and for these specific tests, about 10 s; the signal is therefore shifted by 10 s in order to align it with the other physiological traces and the fMRI scans. Low-pass filtering was carried with the same FIR filter used for cardiac and respiratory traces, with a cutoff frequency of $f_c = 0.5$ Hz.

2.9. GLM regressors

The procedure to obtain a regressor that reflects that impact of HR in the BOLD timecourse follows closely the one introduced by Shmueli et al. [20]. It begins by defining the HR as $HR(t_n) = \frac{1}{t_{n+1}-t_n}$, where t_n are the time points corresponding to maximum peaks.nAfter this, spurious (outliers) time points were removed from the signal (by linear interpolation of the time points more than 1.96 standard deviations away from the median). A low-pass Gaussian filter with standard deviation $\sigma = 1$ mm was then applied to smooth the data, followed by interpolation to match the middle time point of each fMRI volume.

Following Chang et al. [5], who proposed a robust approach for the estimation of RVT, I computed the root-mean-square (RMS) average fluctuation over a window rather than a peak-to-peak difference originally proposed by [3]. Based on this approach, the standard deviation of the respiratory waveform was computed on a 5 s sliding window (corresponding to 2 TRs) centered at each time point. Additionally, to account for outliers and increase the overall confidence of the estimation (although at the cost of being slightly more conservative), values more than 1.96 standard deviations away from the median were replaced by spline interpolation. Finally, the signal was low-pass filtered with $f_c = 0.3$ Hz to obtain a smoother trace and time points corre-

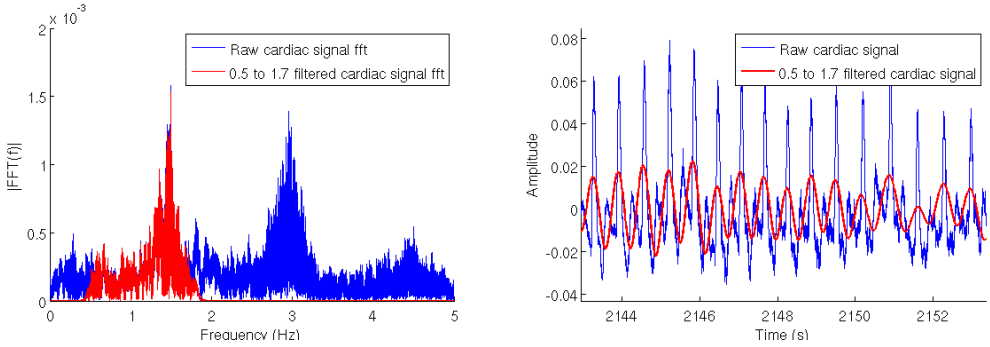

Figure 6: Frequency spectrum of raw and filtered cardiac trace on the left; raw and filtered cardiac time courses on the right.

sponding to the middle of each fMRI acquired volume were extracted to create the corresponding regressor.

In order to use it as a regressor, $P_{ET}CO_2$ was obtained from the the CO_2 trace by simply extracting its peaks, following the procedure found in the literature [12, 22]. To use RR as a regressor, the process is similar to obtaining the heart rate, but starting with the respiratory trace instead of the cardiac trace.

2.10. Response functions

To accurately depict the information carried by the BOLD signal, regressors of the GLM model usually have to be convolved with some sort of response function. For the BOLD response to neuronal activation, this is called the haemodynamic response function (HRF), and it represents the BOLD activation mechanism that the physiological activities previously mentioned have an effect on. The one used in this work for the task-related and the RR regressors was the canonical HRF, i.e., double-gamma HRF with a zero phase. For the HR, RVT and $P_{ET}CO_2$, custom waveforms were defined, attempting to better depict the relationship between these signals and the changes caused in the BOLD mechanism. These were based on the literature, specifically in the ones obtained by Golestani et al. [12], that parametrized them for the three physiological traces (cardiac, respiratory, CO_2) as a double-gamma (see eq 4) and used a deconvolution process to obtain the parameters (see Table 2).

$$h(t) = at^b e^{-\frac{t}{c}} + dt^e e^{-\frac{t}{f}} \quad (4)$$

	a	b	c	d	e	f
HR	0.28	2.42	1.74	-3.46e^{-12}	18.13	0.63
RVT	0.009	2.39	15.22	-1.07e^{-6}	6.44	4.65
$P_{ET}CO_2$	0.20	2.02	3.10	8.80e^{-12}	23.65	0.31

Table 2: Custom parameters for the HRF of each regressor (equation 4).

2.11. GLM fitting

The following GLM's were fitted to the data using FSL's tool:a first analysis performed considered that Action 1 and Action 2 of each task were the variables of interest, while HR, RVT and $P_{ET}CO_2$ were the confounds; and a second set of analysis was performed, replacing the task-related regressors with the respiratory rate. For each GLM and contrast, a statistical parametric map (SPM) of the significant BOLD signal changes associated with the regressors of interest was obtained by cluster thresholding, using voxel Z threshold = 2.3 and cluster P threshold = 0.05., using FSL's tools.

3. Results and discussion

The maps of BOLD signal activations for task-related regressors are not presented, since there were no relevant clusters, as said in section 3.2.

3.1. Consistency of physiological measurements

The physiological variables HR, RR and $P_{ET}CO_2$ were averaged across the 30 s period of each task, according to the protocol design described in Section 2.1, and shown in Table 1. The percentual

increase in the averages of the results for two data sets (BS's PB2 and KS's PB2) can be seen in Figure 7, along with a black line plotted in an effort to visualize possible trends present in the graphs.

For the HR regressor of the BS subject, there is a marked decrease on average when going from one of the two actions to the baseline, and there is almost no change for $P_{ET}CO_2$ regressor of the same subject, when going from baseline into Action 2. In the KS subject, the HR regressors behaves similarly to the one from BS, but with less marked decreases going to the baseline, and larger increases when going to Action 2. The $P_{ET}CO_2$ regressor in this case shows no discernible trend or pattern. In both cases it is the RR regressor that shows the greater percentual changes. And while in the BS case there is no discernible trend or pattern, in the KS case there is a very large increase when going from baseline into Action 2, and a very large decrease when going from Action 2 into baseline. Relatively to these changes, going into Action 1 provokes very little changes in the RR regressor. This suggests that the volunteers did not comply to the protocol.

3.2. Maps of BOLD activity related with respiratory tasks

The first analysis performed considered that Action 1 and Action 2 of each task were the variables of interest, while HR, RVT and $P_{ET}CO_2$ were the confounds. These maps showed almost no activation in the brainstem for any case, and only some cortical activity for BS's PB2 and KS's NG, probably due to the task-related regressors not being an accurate way of portraying the changes in the BOLD signal, since the volunteers did not comply, as seen in the previous section.

3.3. Maps of BOLD activity related with RR

Another GLM analysis was run replacing the task-related regressors with the RR. The main results obtained with this contrast can be seen in Figures 3, 4 and 5.

Figure 3 shows some consistent activity in the middle dorsal areal of the brainstem, over the boundary between brainstem and cerebellum, possibly identifiable as the dorsal raphe, which was first identified in an fMRI analysis by Bianciardi et al [1], and is one of the nuclei responsible for eliciting motor action that leads to respiration , in response to stimulus provided by the nuclei in the pons, most notably by the pneumotaxic center. Figures 4 and 5 show some cortical activity in the frontal and temporal lobes, precisely the cortical areas related to problem solving and cognitive loading, as was expected to see in the NG task, but not in the PB2 task. Figure 4 also presents a significant cluster located in the middle of the pons, possibly atributting it to the pneumotaxic center, while Figure 5 shows no significant activation in the brainstem.

4. Conclusions

The results of this work are somewhat promising, but not entirely conclusive. The results appear to indicate that it is indeed possible to correctly individualize respiratory nuclei activity in the brainstem, but the process needs optimization and generalization to have statistical significance. This means that although not providing conclusive results, this work provides clear enough indications of a path to follow regarding these questions, and enough evidence of the work already being set in the right direction.

Finally, this can be transposed to some future work guidelines: implementing a more complete and robust processing pipeline for both the image and physiological data; specially including the lag optimization of the regressors sync with the BOLD signal; extending the study to more subjects in order to allow for statistically significant group analysis; the response functions used for the regressors also deserve more study, so as to optimize them to the data, possibly using the deconvolution approach used by Golestani et al [12]; and possibly using another derivation of respiratory activity as a confound, and using both the RR and the RVT as variables of interest. These final remarks leave the way open for further research in the topic and in this specific protocol, with the objective of experimentally observe and understand the modulation of the BOLD signal by respiratory activity.

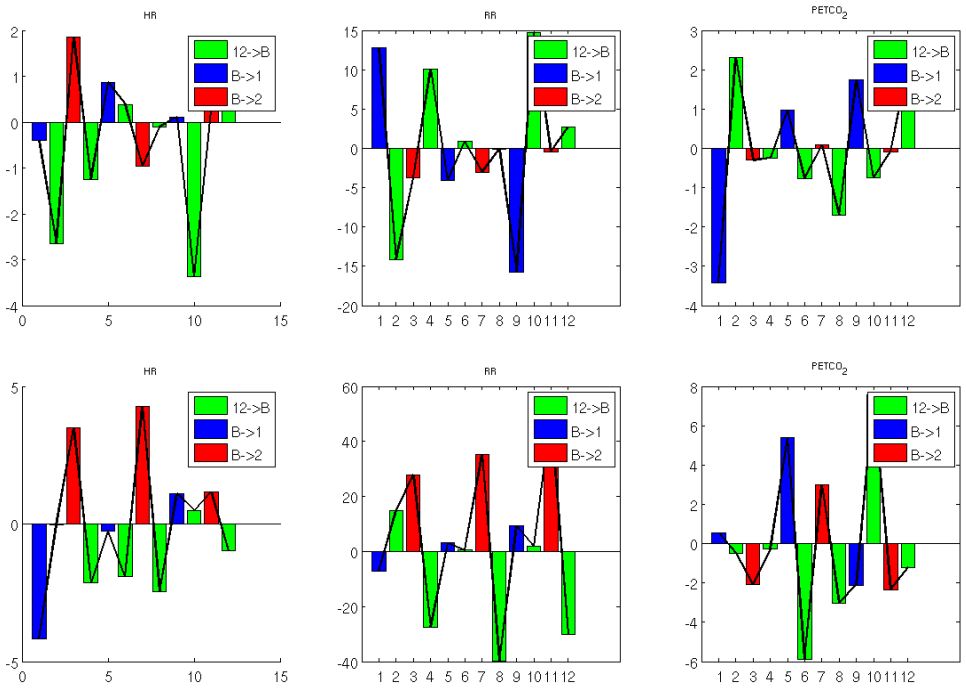

Figure 7: HR (left), RR (center) and $P_{ET}CO_2$ (right) percentual increase in the averages across 30 s periods corresponding to the PB2 task periods (A1, B, A2), relative to the previous period; upper row is relative to subject BS, lower row is relative to subject KS. A black line following the bars' values in the center of the bars is plotted in black.

References

[1] M. Bianciardi, N. Toschi, B. L. Edlow, C. Eichner, K. Setsompop, J. R. Polimeni, E. N. Brown, H. C. Kinney, B. R. Rosen, and L. L. Wald. Toward an in vivo neuroimaging template of human brainstem nuclei of the ascending arousal, autonomic, and motor systems. *Brain connectivity*, 5(10):597–607, 2015.

[2] R. M. Birn. The role of physiological noise in resting-state functional connectivity. *Neuroimage*, 62(2):864–870, 2012.

[3] R. M. Birn, J. B. Diamond, M. A. Smith, and P. A. Bandettini. Separating respiratory-variation-related fluctuations from neuronal-activity-related fluctuations in fmri. *Neuroimage*, 31(4):1536–1548, 2006.

[4] R. B. Buxton. *Introduction to functional magnetic resonance imaging: principles and techniques*. Cambridge university press, 2009.

[5] C. Chang, J. P. Cunningham, and G. H. Glover. Influence of heart rate on the bold signal: the cardiac response function. *Neuroimage*, 44(3):857–869, 2009.

[6] C. Chang and G. H. Glover. Relationship between respiration, end-tidal co 2, and bold signals in resting-state fmri. *Neuroimage*, 47(4):1381–1393, 2009.

[7] E. A. DeYoe, P. Bandettini, J. Neitz, D. Miller, and P. Winans. Functional magnetic resonance imaging (fmri) of the human brain. *Journal of neuroscience methods*, 54(2):171–187, 1994.

[8] K. C. Evans, D. D. Dougherty, A. M. Schmid, E. Scannell, A. McCallister, H. Benson, J. A. Dusek, and S. W. Lazar. Modulation of spontaneous breathing via limbic/paralimbic–bulbar circuitry: An event-related fmri study. *Neuroimage*, 47(3):961–971, 2009.

[9] J. L. Feldman and C. A. Del Negro. Looking for inspiration: new perspectives on respiratory rhythm. *Nature Reviews Neuroscience*, 7(3):232–241, 2006.

[10] J. L. Feldman, C. A. Del Negro, and P. A. Gray. Understanding the rhythm of breathing: so near yet so far. *Annual review of physiology*, 75:423, 2013.

[11] W. Ganong. *Review of Medical Physiology*. USA: appleton & Lange, 1999, 1999.

[12] A. M. Golestani, C. Chang, J. B. Kwinta, Y. B. Khatamian, and J. J. Chen. Mapping the end-tidal co 2 response function in the resting-state bold fmri signal: spatial specificity, test–retest reliability and effect of fmri sampling rate. *Neuroimage*, 104:266–277, 2015.

[13] K. Ikeda, K. Kawakami, H. Onimaru, Y. Okada, S. Yokota, N. Koshiya, Y. Oku, M. Iizuka, and H. Koizumi. The respiratory control mechanisms in the brainstem and spinal cord: integrative views of the neuroanatomy and neurophysiology. *The Journal of Physiological Sciences*, pages 1–18, 2016.

[14] M. Jenkins, C. Beckmann, T. Behrens, M. Woolrich, and S. Smith. Fsl. *Neuroimage*, 62:782–90, 2012.

[15] P. Jezzard, P. M. Matthews, and S. M. Smith. *Functional MRI: an introduction to methods*. Oxford university press, 2001.

[16] G. Krüger and G. H. Glover. Physiological noise in oxygenation-sensitive magnetic resonance imaging. *Magnetic resonance in medicine*, 46(4):631–637, 2001.

[17] S. Nunes. Characterization of physiological noise in resting-state fmri data at 7t. Master's thesis, Instituto Superior Técnico, 2014.

[18] D. Raj, A. W. Anderson, and J. C. Gore. Respiratory effects in human functional magnetic resonance imaging due to bulk susceptibility changes. *Physics in medicine and biology*, 46(12):3331, 2001.

[19] Q. Shen, H. Ren, and T. Q. Duong. Cbf, bold, cbv, and cmro2 fmri signal temporal dynamics at 500-msec resolution. *Journal of Magnetic Resonance Imaging*, 27(3):599–606, 2008.

[20] K. Shmueli, P. van Gelderen, J. A. de Zwart, S. G. Horovitz, M. Fukunaga, J. M. Jansma, and J. H. Duyn. Low-frequency fluctuations in the cardiac rate as a source of variance in the resting-state fmri bold signal. *Neuroimage*, 38(2):306–320, 2007.

[21] S. M. Smith, M. Jenkinson, M. W. Woolrich, C. F. Beckmann, T. E. Behrens, H. Johansen-Berg, P. R. Bannister, M. De Luca, I. Drobnjak, D. E. Flitney, et al. Advances in functional and structural mr image analysis and implementation as fsl. *Neuroimage*, 23:S208–S219, 2004.

[22] I. Sousa, P. Vilela, and P. Figueiredo. Reproducibility of hypocapnic cerebrovascular reactivity measurements using bold fmri in combination with a paced deep breathing task. *NeuroImage*, 98:31–41, 2014.

[23] A. J. van der Kouwe, T. Benner, D. H. Salat, and B. Fischl. Brain morphometry with multiecho mprage. *Neuroimage*, 40(2):559–569, 2008.

[24] A. Webb and G. C. Kagadis. Introduction to biomedical imaging. *Medical Physics*, 30(8):2267–2267, 2003.

[25] R. G. Wise, K. Ide, M. J. Poulin, and I. Tracey. Resting fluctuations in arterial carbon dioxide induce significant low frequency variations in bold signal. *Neuroimage*, 21(4):1652–1664, 2004.

[26] K. J. Worsley, C. Liao, J. Aston, V. Petre, G. Duncan, F. Morales, and A. Evans. A general statistical analysis for fmri data. *Neuroimage*, 15(1):1–15, 2002.